Anti-Axl monoclonal antibodies attenuate the migration of MDA-MB-231 breast cancer cells

HONG CHANG[1,2*], RAN AN[2,3*], XINYING LI[4], XIAOLING LANG[5], JIANNAN FENG[4,5] and MING LV[5,6]

[1]Institute of Medical Technology, Suzhou Vocational Health College, Suzhou, Jiangsu 215009; [2]College of Basic Medicine, Hebei University of Chinese Medicine, Shijiazhuang, Hebei 050200; [3]Hebei Key Laboratory of Chinese Medicine Research on Cardio-cerebrovascular Disease, Hebei University of Chinese Medicine, Shijiazhuang, Hebei 050051; [4]State Key Laboratory of Toxicology and Medical Countermeasures, Beijing Institute of Pharmacology and Toxicology; [5]Beijing Key Laboratory of Therapeutic Gene Engineering Antibody; [6]Laboratory of Immunology, Institute of Military Cognitive and Brain Sciences, Beijing 100850, P.R. China

Received April 29, 2021; Accepted July 26, 2021

DOI: 10.3892/ol.2021.13010

Abstract. The receptor tyrosine kinase, anexelekto (Axl) is involved in tumor cell growth, migration and invasion, and has been associated with chemotherapy resistance, which makes it an attractive target for cancer therapy. In total, six Axl-targeted monoclonal antibodies (mAbs) and two antibody-drug conjugates have been reported in the last 10 years, which have been shown to have bioactivity in inhibiting tumor cell proliferation and migration. The Axl external cell domain (Axl^{-ECD}), consisting of 426 amino acids, has always been used as an antigen in the screening process for all six of these Axl-targeted mAbs. However, the Axl functional domain, which interacts with its natural ligand, growth arrest-specific protein 6 (Gas6), is only a small part of the Axl^{-ECD}. Antibodies targeting the Axl functional domain may efficiently block Gas6-Axl binding and attenuate its downstream signals and activities. To the best of our knowledge, no mAbs targeting the Axl functional domain have been reported. In the present study, a major Axl functional domain interacting with Gas6 was determined using bioinformatics and structural biology methods. In MDA-MB-231 breast cancer cell assays, anti-Axl mAbs targeting this relatively specific Axl functional domain almost completely neutralized the stimulation of Gas6 in both Axl phosphorylation and cell migration assays, and showed similar activity to the positive control drug R428 (a small molecular tyrosine kinase inhibitor of Axl currently in phase II clinical trials) in the cell migration assay. Given the important role of Axl in tumor development and chemotherapy resistance, Axl-targeted mAbs could be used to inhibit tumor cells directly, as well as reduce the development of chemotherapy resistance by blocking Axl activity. The application of Axl-targeted mAbs combined with chemotherapy provides a promising treatment strategy for patients with tumors, particularly those with triple-negative breast cancer, for whom no targeted therapy is currently available.

Correspondence to: Professor Ming Lv, Laboratory of Immunology, Institute of Military Cognitive and Brain Sciences, 27 Taiping Road, Beijing 100850, P.R. China
E-mail: lm62033@163.com

Professor Jiannan Feng, State Key Laboratory of Toxicology and Medical Countermeasures, Beijing Institute of Pharmacology and Toxicology, 27 Taiping Road, Beijing 100850, P.R. China
E-mail: fengjiannan1970@qq.com

*Contributed equally

Abbreviations: Gas6, growth arrest-specific protein 6; mAb, monoclonal antibody; Axl^{-ECD}, Axl external cell domain; Axl^{-ECD}-Fc, Axl^{-ECD} fused with IgG1-Fc; Axl^{-Ig1}, Axl Ig-like domains 1; $Gas6^{-LG1}$, Gas6 laminin G-like domain 1; TNBC, triple-negative breast cancer; NSCLC, non-small cell lung cancer; IPTG, isopropyl-β-D-thiogalactopyranoside; HAT, hypoxanthine/aminopterin/thymidine

Key words: Axl, Axl functional domain, anti-Axl mAb, Axl signaling, breast cancer cells, cell migration

Introduction

Anexelekto (Axl), a member of the Tyro3, Axl and Mertk family of receptor tyrosine kinases (RTKs), can be activated by phosphorylation from binding of its natural ligand, growth arrest-specific protein 6 (Gas6), and has been associated with tumor cell growth, migration, invasion and immune suppression (1-5). Upregulation or overactivation of Axl has been reported in various solid tumors, leukemias and other types of lymphoid neoplasms, particularly in invasive types of cancer (1-3,6-8).

More importantly, chemotherapy can indirectly induce the upregulation and phosphorylation of Axl, which may trigger cell survival signaling and, ultimately, contribute to chemoresistance in breast, colon, lung cancer, mesothelioma and acute myeloid leukemia (2,4,9-11). By contrast, inhibition of Axl can reduce tumor cell proliferation and migration, as well as maintain the sensitivity of tumor cells to chemotherapeutic agents (12-14). Therefore, the

critical role of Axl in tumor development, progression and therapeutic resistance makes it an attractive target for cancer therapy (2,8,15).

Small molecular tyrosine kinase inhibitors and monoclonal antibodies (mAbs) are the main Axl inhibitors. A total of 26 small molecular kinase inhibitors against Axl have been reported to date, and have either been proven or are under clinical and preclinical development (4,5,15,16). However, most of these kinase inhibitors target several RTKs sharing similar kinase domains and, generally, Axl is not the primary target (2,4,15). In total, only three kinase inhibitors have Axl as their selective target (5). R428 (BGB324) is the first selective kinase inhibitor to target Axl only and is currently undergoing phase II clinical trials (4,5,16-18).

Compared with smaller molecular kinase inhibitors, research into Axl-targeted mAb has developed more recently. In total, six groups of Axl-targeted mAbs (DAXL-88, 20G7-D9, AXL antibody, D9/E8, YW327.6S2 and 3G9/8B5/12A11/4F8) have been reported during the last 10 years. These mAbs have shown bioactivity in blocking the Gas6-Axl interaction and downstream signaling (1,3,6,19), inhibiting tumor cell proliferation and migration (3,6,7,12), attenuating tumor xenograft growth (1,3,6,19) and reducing the invasion of cancer cells (1,19) in studies examining triple-negative breast cancer (TNBC), non-small cell lung cancer (NSCLC) and pancreatic cancer models. In addition, two antibody-drug conjugates (Enapotamab vedotin and BA3011) have been reported (20,21). The development of Axl inhibitors was our main focus, and we investigated a phage-derived human mAb (DAXL-88) and variants of the Axl external cell domain (Axl^{-ECD}) fused with IgG1-Fc (Axl^{-ECD}-Fc) (3,22).

In antibody research, the design and preparation of the antigen are the most important steps for screening functional mAbs. For the aforementioned six groups of Axl-targeted mAbs, the Axl^{-ECD} was used as the antigen in the screening process. The Axl^{-ECD} [26-451 amino acids (aa)] consists of 426 aa, and the Axl functional domain, that interacts with Gas6, is only a small component of Axl^{-ECD}. Antibodies targeting the Axl functional domain may efficiently block Gas6-Axl binding and attenuate downstream signals and activities. To the best of our knowledge, no mAb that targets the Axl functional domain has been previously reported.

In the present study, the major Axl functional domain, interacting with Gas6, was determined using bioinformatics and structural biology methods. Subsequently, anti-Axl mAbs were generated using hybridoma technology and evaluated using a series of biological experiments.

Materials and methods

Reagents and antibodies. The pGEX-4T-1-Axl^{-Ig1} recombinant plasmid was purchased from Beijing SinoGenoMax Research Center Co., Ltd. The Axl^{-ECD}-Fc was made in our laboratory (Beijing Key Laboratory of Therapeutic Gene Engineering Antibody, Beijing, China). The biotin-labeled Axl^{-ECD}-Fc was purchased from Beijing Jiaxuan Zhirui Biotechnology Co., Ltd. RPMI-1640 medium (cat. no. A1049101), DMEM (cat. no. C11995500BT), 0.25% trypsin-EDTA (cat. no. 25200-072) and FBS (cat. no. 1997802C) were purchased from Gibco (Thermo Fisher Scientific, Inc.). Freund's complete adjuvant (cat. no. F5881), Freund's incomplete adjuvant (cat. no. F5506), polyethylene glycol (PEG1450; cat. no. P7306) and hypoxanthine-aminopterin-thymidine (HAT) media supplement (cat. no. H0262) were purchased from Sigma-Aldrich (Merck KGaA). Escherichia coli BL21 (DE3) competent cells (cat. no. C1400), Glutathione S-transferase (GST) beads (cat. no. P2020), RIPA buffer (cat. no. R0010) and Giemsa solution (cat. no. G1010) were purchased from Beijing Solarbio Science and Technology Co., Ltd. HiTrap Protein G HP (cat. no. 17-0405-01) was purchased from GE Healthcare (Cytiva). R428 inhibitor (cat. no. CC2997) was purchased from ChemCatch (http://www.chemcatch.cn/index.php). The 3,3',5,5,-tetramethylbenzidine (TMB) solution (cat. no. 00-4201-56) was purchased from Invitrogen (Thermo Fisher Scientific, Inc.).

Recombinant human Gas6 protein (cat. no. 885-GSB) and goat anti-Axl polyclonal antibody (cat. no. AF154) were purchased from R&D Systems, Inc. Anti-phosphorylated (p)-Axl (cat. no. 5724), anti-mouse IgG-HRP (cat. no. 7076), anti-rabbit IgG-HRP (cat. no. 7074) and anti-GAPDH-HRP (cat. no. 51332) antibodies were purchased from Cell Signaling Technology, Inc. Streptavidin-HRP (cat. no. 554066) was purchased from BD Biosciences. Anti-mouse IgG-FITC (cat. no. ab6785), anti-goat IgG-FITC (cat. no. ab6737) and anti-goat IgG-HRP (cat. no. ab6741) were purchased from Abcam. Goat anti-human IgG (GAH-IgG; cat. no. 01-10-06) was purchased from KPL, Inc., while mouse anti-GST IgG (cat. no. 66001-2-Ig) was purchased from ProteinTech Group, Inc.

Animals. A total of 4 female BALB/c mice were purchased from JOINN Laboratories. The animal experiments were approved by the Animal Ethics Committee of Suzhou Vocational Health College (Jiangsu, China; approval no. SWAE201905) and performed in accordance with the Guidelines of the Care and Use of Laboratory Animals of the Ministry of Health, China to minimize animal suffering and distress. The mice were monitored daily by an animal keeper and no mice died during the experiment. The mice were anesthetised with 2% isoflurane and blood was extracted from the tails to verify the immune titer. A total of 4 mice were euthanized by cervical dislocation and death was verified by respiratory and cardiac arrest. The duration of the experiment was 8 weeks and 3 days.

Cell culture. The human breast cancer cell line, MDA-MB-231 (cat. no. HTB-26) and the human NSCLC cell line H1299 (cat. no. CR-5803) were purchased from the American Type Culture Collection and were authenticated by Beijing ZhongYuan Ltd., in 2014. The SP2/0 mouse myeloma cell line (cat. no. CL-0217) was purchased from Procell Life Science&Technology Co.,Ltd. The cells were cultured in DMEM containing 10% FBS and 100 U/ml penicillin-streptomycin at 37˚C in a humidified incubator with 5% CO_2.

Bioinformatics. The protein sequence information for Axl (UniProtKB P30530) was determined using www.ebi.ac.uk. The crystal complex information for Gas6-Axl (no. 2C5D) was obtained from the Protein Data Bank (https://www.ncbi.nlm.nih.gov/Structure/pdb). Interaction analysis of Gas6-Axl was performed using Insight II 2000 software (Insight Software, Inc.).

Interaction analysis between Axl and Gas6. Theoretical analyses were performed as described in our previous study (22). Briefly, based on the crystal complex structure (23), the Gas6-Axl theoretical complex model was constructed and optimized using the steepest decent and conjugate gradient method (discovery mode) under the consistent valence force field. With the optimized complex structure, the computer graphics technique and the distance geometry method (standard mode) were used to analyze the Gas6-Axl interaction mode. The superimposition method (standard mode) was used to identify the orientation of the main chain carbon atoms. Furthermore, the interaction binding free energy calculation method (discovery mode) was used to calculate the binding energy of Gas6-Axl.

Preparation and identification of the GST-Axl^{-Ig1} antigen. The DNA sequence encoding the Axl functional domain (Axl^{-Ig1}) was confirmed by BLAST analysis (https://blast.ncbi.nlm.nih.gov/Blast.cgi, GenBank: BC032229.1) and cloned into the pGEX-4T-1 vector between *Bam*HI and *Xho*I restiction sites, which allowed for the addition of a GST tag to the N-terminus of the Axl^{-Ig1} domain (GST-Axl^{-Ig1} fusion protein). The recombinant plasmid pGEX-4T-1-Axl^{-Ig1} was transformed into *Escherichia coli* BL21 (DE3) competent cells. After optimization of the expression conditions, the GST-Axl^{-Ig1} fusion protein expression was induced by the addition of 1 mM isopropyl-β-D-thiogalactopyranoside (IPTG) at 20˚C for 6 h, followed by purification using GST beads according to the manufacturer's instructions. Then, the GST-Axl^{-Ig1} fusion protein was analyzed using 12% SDS-PAGE and further validated using western blot analysis and the goat anti-Axl polyclonal antibody, AF154 and mouse anti-GST IgG, as separate primary antibodies, followed by anti-goat IgG-HRP and anti-mouse IgG-HRP as separate secondary antibodies.

Animal immunization and cell fusion. Animal immunization was performed as described previously (24). Briefly, four BALB/c female mice (8-week-old, 18-20 g) were subcutaneously immunized with 100 μg GST-Axl^{-Ig1} antigen in Freund's complete adjuvant on the first week, and in Freund's incomplete adjuvant on the fourth and sixth week. When the immune titer was >1:10,000, the mice were intravenously immunized with 100 μg GST-Axl^{-Ig1} antigen without adjuvant for the final boost. Then, 3 days later, the mice were euthanized by cervical dislocation and the spleen cells from the immunized mice were fused with SP2/0 mouse myeloma cells at a ratio of 7:1 with PEG1450. The fused cells were cultured in RPMI-1640 medium with 20% FBS and HAT, then screened using ELISA and the hybridoma cell supernatant.

Screening of hybridoma cells and production of anti-Axl mAbs. The hybridoma cell clones that bound to GST-Axl^{-Ig1}, but not GST were further screened using a BD FACSCalibur™ flow cytometer (cat. no. 342975; BD Biosciences) and FlowJo software (version 7.6; BD Biosciences) using H1299 cells (NSCLC cell line) with a high expression of Axl. The H1299 cell line was incubated with the hybridoma cell supernatant containing anti-Axl mAbs and detected using anti-mouse IgG-FITC (1:1,000). Goat anti-Axl polyclonal antibody AF154 (1:500) served as a positive control and was detected using anti-goat IgG-FITC (1:1,000). ELISAs were always performed before flow cytometry screening. After three rounds of ELISA, flow cytometry and limited dilution subclonal screening, hybridoma cell secreting anti-Axl mAbs were obtained. The hybridoma cells were cultured at 37˚C with 5% CO_2, and $3x10^6$ hybridoma cells ($6x10^6$ cells/ml) were seeded into the abdominal cavity of each mouse to boost the production of the antibody protein. Anti-Axl mAbs were purified from the mouse ascites using Protein G affinity chromatography and an ÄKTAprime® plus system (cat. no. 11001313; Cytiva) with 20 mM sodium phosphate (pH 7.0) as binding buffer, and 0.1 M glycine-HCl (pH 2.7) as elution buffer according to the manufacturer's instructions. Anti-Axl mAbs were analyzed via reduced and non-reduced 12% SDS-PAGE, filtered under sterile conditions and stored at 4˚C in PBS. Protein concentrations were determined using a BCA kit (Applygen Technologies, Inc.).

Binding to Axl fusion proteins (measured using ELISA). The anti-Axl mAbs were tested for binding with Axl fusion proteins, Axl^{-ECD}-Fc and GST-Axl^{-Ig1}. The ELISA plates were coated with 2 μg/ml Axl^{-ECD}-Fc and GST-Axl^{-Ig1} in 0.1 M sodium carbonate buffer (pH 9.6) overnight at 4˚C. After blocking with 10% FBS in PBS buffer at 37˚C for 1 h, the plates were incubated with serial dilutions of mouse anti-Axl mAb (5.56, 1.85, 0.62, 0.21, 0.069, 0.023, 0.008, 0.0027 and 0.0009 μg/ml) at 37˚C for 1 h. Subsequently, anti-mouse IgG-HRP (1:2,500) was added as the secondary antibody and incubated at 37˚C for 30 min. The binding signals were visualized using the TMB substrate and the absorbance was measured at 450 nm using a SPECTRA MAX 190 ELISA reader (Molecular Devices, LLC). The ELISA plates were separately washed with TBS-Tween-20 (TBST; 50 mM Tris-HCl, 150 mM NaCl, 0.2% Tween-20, pH 7.4) three times for 5 min after coating, blocking and incubating with the primary and secondary antibodies.

Binding to Axl proteins (measured using western blot analysis). The anti-Axl mAbs were tested for binding to the Axl fusion proteins. Axl^{-ECD}-Fc and GST-Axl^{-Ig1} proteins were resolved on 12% SDS-PAGE and transferred onto a PVDF membrane, which was blocked with 5% skimmed milk at room temperature for 1 h. The membranes were incubated with mouse anti-Axl mAbs (10 μg/ml) overnight at 4˚C, then with anti-mouse IgG-HRP (1:2,500) at room temperature for 1 h. The anti-Axl polyclonal antibody AF154 (1:500) was used as the positive control to recognize the Axl^{-ECD} and Axl^{-Ig1} domains and was detected using the anti-goat IgG-HRP (1:2,500). Finally, the membranes were developed using an ECL detection system (SuperSignal Westpico Trial kit; Thermo Fisher Scientific, Inc.). The membrane was separately washed three times with TBST for 10 min after transferring, blocking and incubating with the primary and secondary antibodies.

The anti-Axl mAbs were tested for binding to Axl molecules on the surface of the cells. After trypsin digestion, the MDA-MB-231 cell lysates from $5x10^5$ cells were obtained using ice-cold RIPA buffer and were resolved using 12% SDS-PAGE. The subsequent steps were the same as aforementioned. The anti-Axl antibody AF154 was also used as the positive control.

Flow cytometry. After trypsin digestion, $3x10^5$ MDA-MB-231 cells were collected and incubated with mouse anti-Axl mAb (10 μg/ml) as the primary antibody at 4˚C for 30 min. The cells were then incubated with anti-mouse IgG-FITC (1:1,000) as the secondary antibody at 4˚C for 30 min. Finally, the cells were detected using a BD FACSCalibur™ flow cytometer (cat. no. 342975; BD Biosciences). The cells were separately washed three times with washing buffer (PBS containing 2% FBS) after digestion and incubation with the primary and secondary antibodies.

Competitive ELISA. ELISA was performed as aforementioned. Briefly, the ELISA plates were coated with 0.5 μg/ml Gas6, and incubated with 2 μg/ml biotin-labelled Axl^{-ECD}-Fc, then with serial dilutions of anti-Axl mAb (500, 125, 32, 8, 2 and 0.5 μg/ml). Streptavidin-HRP (1:1,000) was added as the secondary antibody and binding signals were measured at 450 nm. The ELISA plates were washed three times separately with TBST for 5 min after coating, blocking and incubating with the primary and secondary antibodies.

Detection of Axl and p-Axl proteins using western blot analysis. Western blot analysis was performed as aforementioned. The MDA-MD-231 cells were seeded into 6-well plates at $3x10^5$ cells/well and cultured overnight. After incubation, 100 μg/ml (0.67 μmol/l) anti-Axl mAbs were added to the cells for 4 h, followed by the addition of 200 ng/ml Gas6 for 15 min. Neither Gas6 nor anti-Axl mAbs were added to the non-treated group (NT). Subsequently, the cell lysates were obtained using ice-cold RIPA buffer, and the proteins were resolved on 12% SDS-PAGE after quantification using a BCA kit (Applygen Technologies, Inc.). The proteins were transferred onto a PVDF membrane, followed by blocking with 5% skimmed milk. Goat anti-Axl antibody AF154 (1:500) and anti-goat IgG-HRP (1:2,500) were used to detect the expression level of Axl, and rabbit anti-p-Axl antibody (1:500) and anti-rabbit IgG-HRP (1:2,500) were used for the detection of p-Axl (Tyr702). Finally, the signal was detected using ECL detection reagents and semi-quantified using ImageJ software (version 18.0; National Institutes of Health). The membrane was washed three times with TBST for 10 min after transferring, blocking and incubating with the primary and secondary antibodies.

Transwell migration assay. To assess cell migration, 8-μm pore size BD-Falcon 24 Fluoroblock Transwell inserts were used. After serum-starved culture overnight, $1x10^5$ MDA-MB-231 cells were seeded into the upper chamber containing serum-free DMEM. For Gas6-dependent migration, 200 ng/ml Gas6 was added to the lower chamber containing 10% FBS+ DMEM in the presence or absence of anti-Axl mAbs (100 μg/ml or 0.67 μmol/l). R428 (0.67 μmol/l) was selected as the positive control. Neither Gas6 nor anti-Axl mAbs/R428 were added to the NT group. After 4 h of migration at 37˚C, the non-migrating cells on the top surface of the filter were removed using cotton swabs. The migrating cells on the bottom surface of the filter were fixed with 4% paraformaldehyde for 30 min at room temperature and stained with Giemsa solution for 10 min at room temperature. Images of the migrating cells were captured under a light microscope, then quantified using ImageJ software (version 1.52p; National Institutes of Health), based on five random visual fields in the different groups.

Wound healing assay. After trypsin digestion, $8x10^5$ MDA-MB-231 cells were seeded into 6-well plates in 2 ml DMEM per well. At 90% confluence, wounds were created by scratching the cell monolayer with a sterile p200 μl pipette tip. Then, the cells were washed with PBS and cultured in serum-free DMEM containing anti-Axl mAbs (100 μg/ml or 0.67 μmol/l) or R428 (0.67 μmol/l) as the positive control. In total, five images from random visual fields for each group were captured at 0 and 24 h post-wounding. The wounded area was measured using ImageJ software (version 1.52p; National Institutes of Health), and recorded as S_0 and S_{24} respectively. The cell migration rate (%) was calculated with the following formula: $(S_0-S_{24})/S_0$ x 100%.

Statistical analysis. All assays related to bioactivities were repeated three times. The data were presented as the mean ± SD. Statistical analysis was performed using GraphPad Prism software v.8.0 (GraphPad Software, Inc.). For the Axl, p-Axl level detection and cell migration assays, one-way ANOVA was performed and Dunnett's multiple comparisons test was used to compare all other groups with the Gas6 group or NT group. $P<0.05$ was considered to indicate a statistically significant difference.

Results

Determination of the Axl functional domain. The natural ligand, Gas6, binds to Axl and actives downstream signaling pathways. Thus, the current study first determined the functional domain of Axl that interacts with Gas6, before preparing an antigen containing the specific domain. Schematic representation of the Gas6-Axl interaction is showed in Fig. 1A. The protein sequence information of Axl (UniProtKB P30530) was obtained by searching www.ebi.ac.uk. As shown in Fig. 1A, the Axl protein consisted of 894 aa, with a signal peptide (1-25 aa) and a mature chain (26-894 aa). The mature chain of Axl consisted of an extracellular domain (26-451 aa), a transmembrane region (452-472 aa) and an intracellular domain (473-894 aa). There were two Ig-like domains in the extracellular domain, Axl Ig-like domain 1(Axl^{-Ig1}, 27-128 aa) and Axl Ig-like domain 2 (Axl^{-Ig2}, 139-222 aa).

Based on the crystal complex information (PDB no. 2C5D) (23) and the theoretical complex structure of Gas6-Axl (Fig. 1C), Axl^{-Ig1} (27-128 aa) was determined as the major functional domain interacting with Gas6 using interaction mode analysis and the standard mode. As presented in Fig. 1B, 23 aa residues from Gas6 laminin G-like domains 1 ($Gas6^{-LG1}$) and 22 aa residues from Axl^{-Ig1} interacted at the interface, and resulted in the formation of 13 hydrogen bonds and 120 non-banded contacts between Gas6 and Axl, which was a relatively stable interaction.

It was identified that R^{308}, R^{310}, K^{312}, R^{313} and L^{314} of $Gas6^{-LG1}$ served important roles in interacting with ≥3 aa residues of Axl^{-Ig1} via hydrogen bonds and non-bonded contacts (Fig. 1B), and were considered as the key aa. With respect to Axl^{-Ig1}, E^{56}, E^{59}, D^{73}, S^{74}, T^{75}, Q^{76}, T^{77} and Q^{78} interacted with ≥1 of the key aa

Table I. Amino acids involved in Gas6-Axl interactions.

Study	Interaction	No. of contacts	Gas6^{-LG1}		Axl^{-Ig1}		(Ref.)
			Involved aa	No. of aa		No. of aa	
Sasaki *et al*	Hydrogen bonds	6	R^{299}, S^{302}, $\underline{R^{308}}$, $\underline{R^{310}}$, $\underline{K^{312}}$	5	$\underline{E^{56}}$, $\underline{E^{59}}$, D^{73}, P^{80}	4	(23)
	Other contacts	-	I^{307}, L^{309}, F^{311}, T^{457}, M^{468}, I^{458}, T^{461}	7	T^{75}, $\underline{T^{77}}$, V^{79}, V^{92}, I^{90}	5	
Present study	Hydrogen bonds	13	R^{299}, S^{302}, $\underline{R^{308}}$, $\underline{R^{310}}$, $\underline{K^{312}}$, $\underline{R^{313}}$, $\underline{L^{314}}$, E^{460}	8	$\underline{E^{56}}$, $\underline{D^{73}}$, $\underline{T^{75}}$, P^{80}, R^{48}, $\underline{S^{74}}$, $\underline{Q^{76}}$, $\underline{Q^{78}}$, E^{83},	9	-
	Other contacts	120	I^{307}, L^{309}, F^{311}, T^{457}, M^{468}, M^{300}, T^{304}, P^{305}, V^{306}, R^{414}, L^{416}, D^{455}, T^{456}, N^{465}, S^{663}	15	$\underline{E^{59}}$, $\underline{T^{77}}$, V^{79}, V^{92}, E^{70}, L^{71}, A^{72}, L^{81}, G^{82}, E^{85}, W^{89}, Q^{94}, R^{96}	13	

Data in Italics indicate the aa found in both studies. Underlined data indicate the key aa reported in each study. -, not available. aa, amino acids; Gas6^{-LG1}, Gas6 laminin G-like domains 1; Axl^{-Ig1}, Axl Ig-like domain 1; Axl, anexelekto; Gas6, growth arrest-specific protein 6.

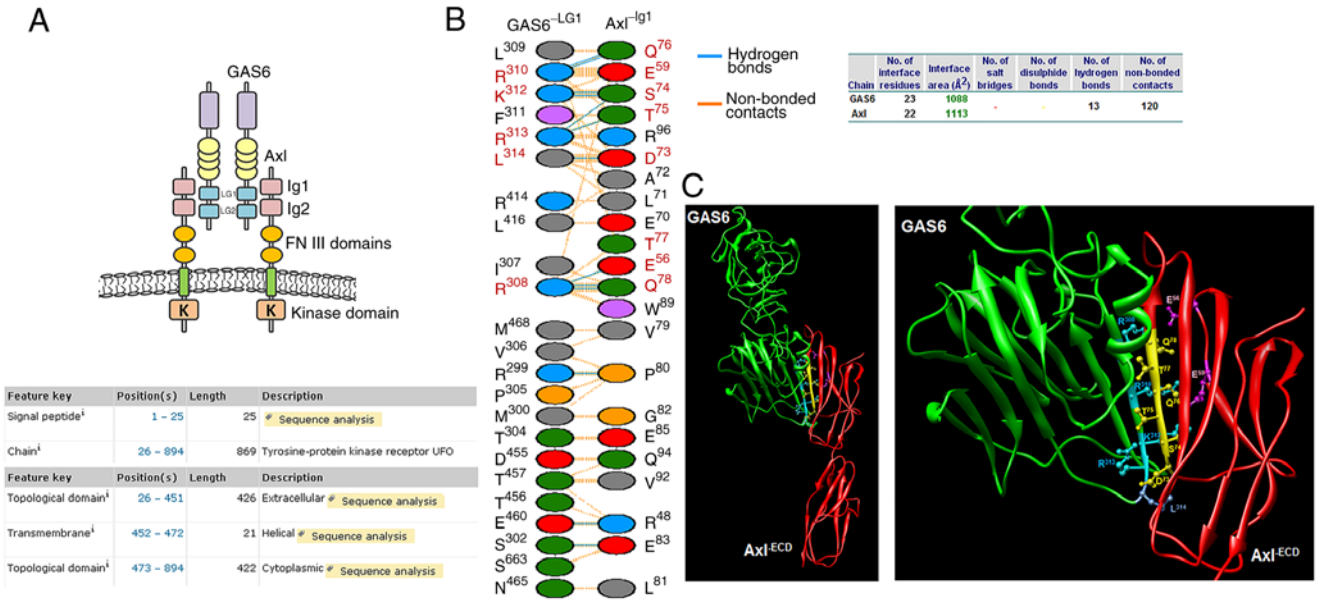

Figure 1. Determination of the Axl functional domain interacting with Gas6. Based on the Gas6-Axl crystal complex structure and the optimized theoretical complex model, theoretical analyses of Gas6-Axl interaction were performed via distance geometry, superimposition and free energy calculation methods using InsightII 2000 software. (A) Schematic representation of Gas6-Axl interaction (up) and amino acid sequence analysis of Axl (down). (B) Interaction mode and interacting amino acid residues at the Gas6-Axl interface. The key amino acid residues were showed in red words. (C) 3-dimentional complex structure of Gas6 and Axl^{-ECD} in overview (left) and in detail (right). Green ribbon, Gas6; red ribbon, Axl^{-ECD}; blue ribbon section, key amino acid residues of Gas6; yellow and pink ribbon sections, key amino acid residues of Axl^{-ECD}. Gas6, growth arrest-specific protein 6; Axl^{-ECD}, Axl external cell domain; Axl, anexelekto.

from Gas6^{-LG1} (Fig. 1B), and were considered as the key aa. Thus, the antibody against this Axl^{-Ig1} domain may block the Gas6-Axl binding and attenuate the downstream signals and bioactivities.

Furthermore, amino acids involved in Gas6-Axl interactions were analyzed and compared between a previous EMBO study (23) and the present study. As presented in Table I, according to Sasaki *et al* (23), 12 aa residues of Gas6^{-LG1} and 9 aa residues of Axl^{-Ig1} were involved in Gas6-Axl interactions, including 6 hydrogen bonds (no data available for the other contacts). Furthermore, 10 aa residues of Gas6 and 8 aa residues of Axl (italicized in Table I) were shared in the study by Sasaki *et al* and the present study. Consistently, R^{308}, R^{310} and K^{312} of Gas6 and E^{56}, E^{59} and T^{77} of the Axl^{-Ig1} domain were considered as the key residues in Gas6-Axl binding by both studies (underlined in Table I). Furthermore, the key role of E^{56}, E^{59} and T^{77} of the Axl^{-Ig1} domain in binding to Gas6 was confirmed by the study by Sasaki *et al* (23) and our previous study using mutants assays (22).

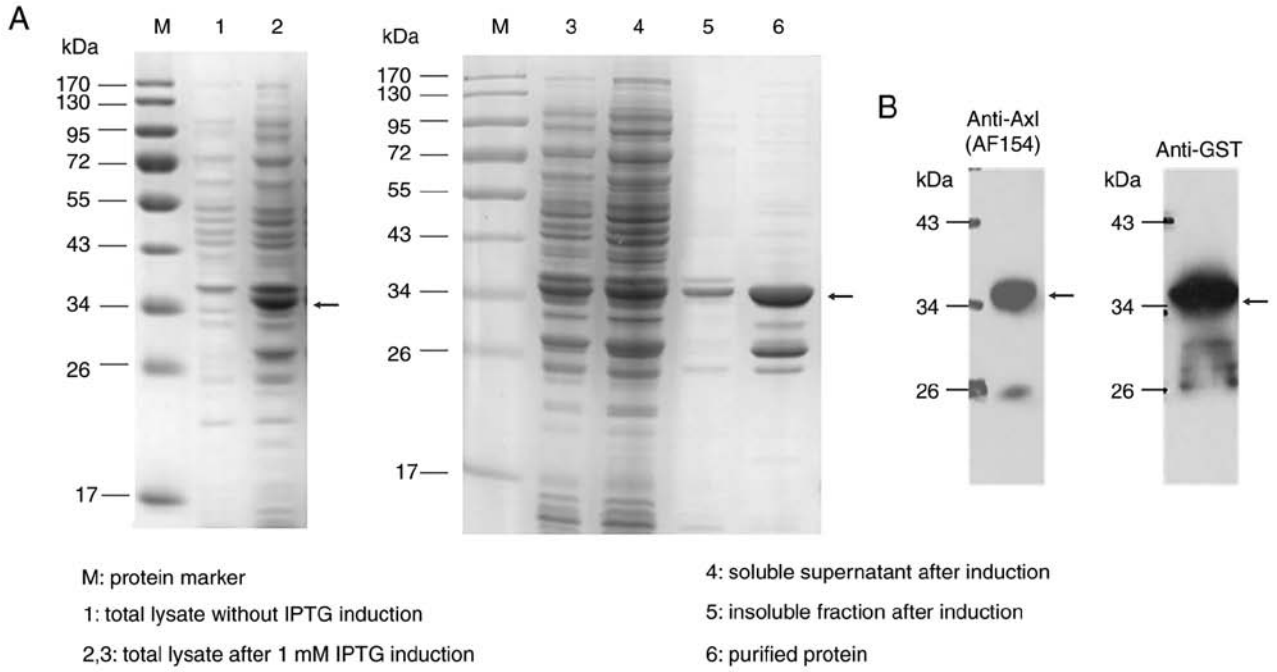

Figure 2. Generation of the GST-Axl^{-Ig1} protein. Western blot analysis of the (A) GST-Axl^{-Ig1} protein and the (B) purified GST-Axl^{-Ig1} protein. The GST-Axl^{-Ig1} protein was validated by incubating with anti-Axl antibody AF154 and anti-GST IgG. M, protein marker; 1, total lysate without IPTG induction; 2 and 3, total lysate after 1 mM IPTG induction; 4, soluble supernatant after induction; 5, insoluble fraction after induction; 6, purified protein. GST, glutathione S-transferase; Axl^{-Ig1}, Axl Ig-like domains 1; Axl, anexelekto; IPTG, isopropyl-β-D-thiogalactopyranoside.

Generation of the GST-Axl^{-Ig1} protein. GST-Axl^{-Ig1} protein expression was induced by 1 mM IPTG at 20˚C for 6 h. As expected, an obvious expression band at 34 kDa was visible after induction following SDS-PAGE analysis, and most of the GST-Axl^{-Ig1} protein was soluble in the ultrasonic supernatant (Fig. 2A). GST-Axl^{-Ig1} protein with high purity was obtained after affinity purification using GST beads. Further western blot analysis revealed that the GST-Axl^{-Ig1} protein could specifically bind with the anti-Axl antibody AF154 and anti-GST IgG (Fig. 2B), indicating that the GST-Axl^{-Ig1} protein was correctly expressed and could be used as an antigen for immunizing animals.

Generation of anti-Axl mAb. In total, seven hybridoma cell clones that bound to GST-Axl^{-Ig1}, but not GST, were selected from six plates of 96-well cells from two rounds of ELISA screening (Fig. 3A) and were further screened using flow cytometry by binding to the H1299 cells with high Axl expression. After three rounds of ELISA and flow cytometry screening in turn, two clones were obtained with 39.42 and 38.80% binding ratio to the H1299 cells, separately (Fig. 3C). Finally, the hybridoma cell clones that specifically bound to the Axl^{-Ig1} functional domain were obtained, named as Am1 and Am2. The two mAbs had the same isotype, IgG3 heavy chain and κ light chain.

After protein G purification, the specific antibody protein bands were observed at ~50 kDa and 25 kDa in reduced SDS-PAGE analysis, and at ~150 kDa in non-reduced SDS-PAGE analysis, and as expected with a high purity (Fig. 3B).

Binding to Axl fusion proteins. As demonstrated by ELISA and western blot analysis (Fig. 4A and B), Am1 or Am2 could bind with the Axl fusion proteins, Axl^{-ECD}-Fc and GST-Axl^{-Ig1}, which indicated that Am1 or Am2 could recognize the Axl^{-ECD} domain and Axl^{-Ig1} functional domain. In the present study, goat anti-human IgG (GAH-IgG) was used as the control for recognizing the human IgG-Fc domain and anti-GST IgG was used as the control for recognizing the GST tag.

Blocking Gas6-Axl interaction. Using competitive ELISA, anti-Axl mAbs were detected for their ability to inhibit Gas6 binding with Axl^{-ECD}-Fc. Biotin-labeled Axl^{-ECD}-Fc and Am1 or Am2 were incubated with the ELISA plates coated with Gas6, and the captured biotin-labeled Axl^{-ECD}-Fc was detected using streptavidin-HRP. As shown in Fig. 4C, the decreasing signal indicated that Am1 and Am2 blocked Axl^{-ECD}-Fc binding to Gas6. Thus, the inhibitory effect of Am1 and Am2 on the Gas6-Axl interaction made it possible to neutralize the activity of Axl. Given that 125 μg/ml Am1 and Am2 had a notable inhibitory effect on the Gas6-Axl interaction, 100 μg/ml Am1 and Am2 was used in the subsequent assays.

Binding to Axl and reducing the levels of Axl and p-Axl. Axl was notably overexpressed in highly invasive cells (1-3,6-8). The anti-Axl mAbs were detected for their binding to the natural Axl proteins on the surface of highly invasive MDA-MB-231 cell using western blot analysis and flow cytometry. As presented in Fig. 5A, Am1 or Am2 could bind to Axl proteins in the cell lysate or on the cell surface.

Gas6 binds to Axl and induces its phosphorylation, which leads to activation of the downstream signaling pathways and the proliferation and migration of tumor cells (2). Axl and p-Axl proteins were detected using western blot analysis to determine the effect of anti-Axl mAb binding with Axl in the MDA-MB-231 cells. For the NT group with no Gas6 stimulation, Axl protein expression was observed at a high level in

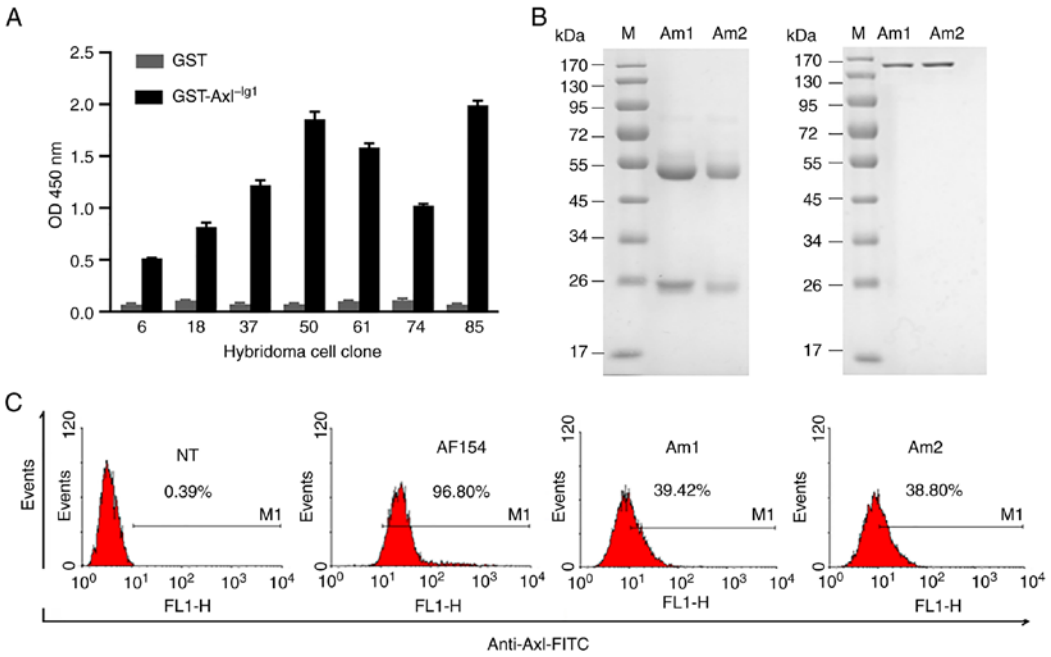

Figure 3. Generation of the anti-Axl mAb. (A) In total, seven positive cell clones, that bound to GST-Axl^{-Ig1} but not GST, were selected by two rounds of ELISA screening. (B) Results of reduced and non-reduced SDS-PAGE analysis of Am1 and Am2 mAbs after protein G purification. (C) A total of seven positive cell clones were further screened using flow cytometry by binding to the H1299 cell line with high expression of Axl. The H1299 cells were incubated with the mouse anti-Axl mAb supernatant and were detected using anti-mouse IgG-FITC. The goat anti-Axl polyclonal antibody, AF154 served as a screening control and was detected using anti-goat IgG-FITC. After three rounds of ELISA and flow cytometry screening, two hybridoma cell clones, that bound specifically to human Axl were obtained, named as Am1 and Am2. NT, non-treated group; mAb, monoclonal antibody; GST, glutathione S-transferase; Axl^{-Ig1}, Axl Ig-like domains 1; Axl, anexelekto.

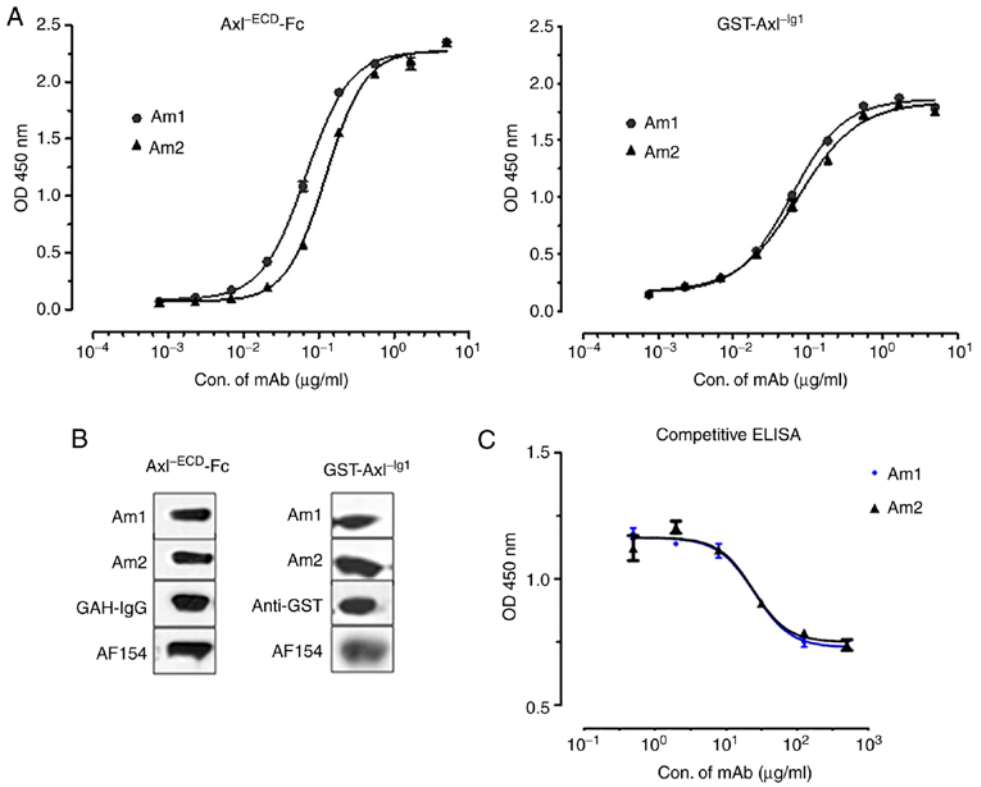

Figure 4. Binding to Axl fusion proteins and blocking Gas6-Axl fusion protein interaction. (A) Am1 or Am2 could bind to Axl fusion proteins, as detected by ELISA. The ELISA plates with Axl^{-ECD}-Fc or GST-Axl^{-Ig1} fusion proteins were incubated with Am1 or Am2 antibody and then detected using anti-mouse IgG-HRP. The error bar in ELISA was too low to be seen. (B) Am1 or Am2 could bind to Axl fusion proteins in the western blot analysis. The PVDF membranes with Axl^{-ECD}-Fc or GST-Axl^{-Ig1} fusion proteins were incubated with Am1 or Am2 antibody and then detected using anti-mouse IgG-HRP. GAH-IgG was used as the control for recognizing the human IgG-Fc domain and anti-GST IgG was used as the control for recognizing the GST tag. (C) Both Am1 and Am2 blocked the Gas6-Axl interaction, as determined by competitive ELISA. ELISA plates were coated with 0.5 μg/ml Gas6 and incubated with biotin-labeled Axl^{-ECD}-Fc and serial dilutions of Am1 or Am2. The captured biotin-labeled Axl^{-ECD}-Fc was detected using streptavidin-HRP. These assays were repeated three times. Gas6, growth arrest-specific protein 6; GST, glutathione S-transferase; Axl^{-Ig1}, Axl Ig-like domains 1; Axl^{-ECD}, Axl external cell domain; Axl^{-ECD}-Fc, Axl^{-ECD} fused with IgG1-Fc; Axl, anexelekto.

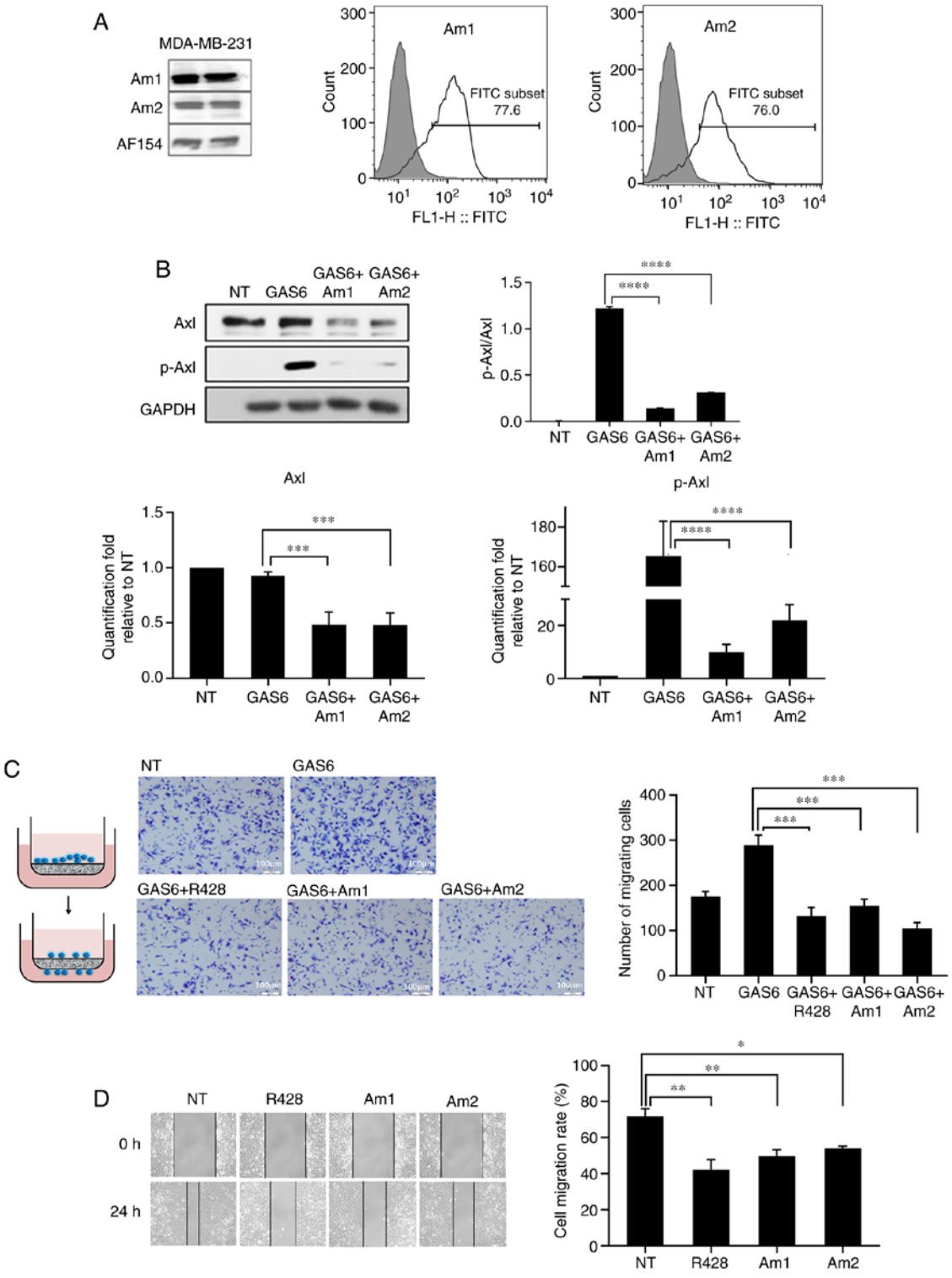

Figure 5. Am1 and Am2 inhibit Axl signaling and cell migration. (A) Am1 or Am2 could bind to the natural Axl protein in the cell lysate or on the cell surface, as determined by western blot and flow cytometry assays. MDA-MB-231 cell lysate or cells were incubated with Am1 or Am2 antibody, then with anti-mouse IgG-HRP or anti-mouse IgG-FITC, separately. (B) Am1 and Am2 reduced the level of Axl and inhibited Axl phosphorylation. MDA-MD-231 cells were incubated with Am1 or Am2 (0.67 μmol/l), followed by 200 ng/ml Gas6 (the NT group was left untreated). GAPDH was used as the loading control. Semi-quantification using ImageJ software of each protein band was normalized to GAPDH and then represented as fold-change relative to the NT group; the ratio of p-Axl/Axl was also shown. (C) Am1 and Am2 attenuated MDA-MD-231 cell migration, as detected in the Transwell assay, with Gas6 (200 ng/ml and either Am1 or Am2 (0.67 μmol/l), or R428 (0.67 μmol/l) as a positive control (the NT group was left untreated). Migrating cells were stained with Giemsa solution, imaged and quantified using ImageJ. (D) Am1 and Am2 attenuated MDA-MD-231 cell migration in the wound-healing assay and the cells were cultured with Am1 or Am2 (0.67 μmol/l), or R428 (0.67 μmol/l) as a positive control, and the results were statistically analyzed. *P<0.05, **P<0.01, ***P<0.001, ****P<0.0001. NT, non-treated group; Gas6, growth arrest-specific protein 6; Axl, anexelekto.

the MDA-MB-231 cells, but p-Axl was almost undetectable (Fig. 5B). Furthermore, Gas6 stimulation for 15 min had no effect on Axl expression but increased p-Axl expression up to 165-fold compared with that in the NT group. It was

also identified that Am1 or Am2 significantly decreased Axl expression from 0.930 to 0.483 or 0.480 folds compared with that in the NT group respectively (P<0.001), and p-Axl expression from 165.35 to 9.99 or 21.91 folds compared with that in the NT group, respectively (P<0.0001). The ratio of p-Axl/Axl is also shown in Fig. 5B. Therefore, it was suggested that Am1 and Am2 could reduce the expression level of Axl and significantly inhibit Axl phosphorylation, which may be the main mechanism preventing tumorigenesis.

Inhibiting cell migration. Anti-Axl mAbs were evaluated for their ability to inhibit cell migration using a Transwell assay. The MDA-MD-231 cells, plated in the upper chamber of Transwell inserts, were stimulated to migrate into the lower chamber containing Gas6 and Am1 or Am2. Compared with that in the Gas6 group, the migration of the MDA-MD-231 cells was significantly attenuated by Am1 or Am2 (P<0.001) to a similar extent as that observed with the Axl inhibitor R428 (P=0.865 and P=0.735, respectively) (Fig. 5C). In addition, cell migration in the Gas6+Am1 or Gas6+Am2 groups was weaker compared with that in the NT group without Gas6 stimulation, indicating that Am1 and Am2 almost completely blocked the stimulation of Gas6.

In the wound healing assay, Am1 or Am2 were added to scratched MDA-MD-231 cells to verify their inhibitory effect on cell migration during the wound healing progress. Compared with that in the NT group, the wound healing speed at 24 h post-wounding was significantly impeded by Am1 (P<0.01) or Am2 (P<0.05), although the inhibitory effect of Am1 or Am2 on cell migration was a little weaker to that observed in the group treated with the Axl inhibitor R428 (Fig. 5D). Collectively, both the Transwell and wound healing assays indicated that Am1 and Am2 could effectively inhibit MDA-MD-231 cell migration.

Discussion

Axl-targeted mAbs have been attracting increasing interest due to the important role of Axl in tumor development and chemotherapy resistance (1,2,4,6,7). Furthermore, accurate determination of the Axl functional domain may make the screening of mAb more effective and feasible. In the present study, Axl^{-Ig1}, consisting of 102 aa, was predicted as the major Axl functional domain interacting with Gas6, based on theoretical analysis of the Gas6-Axl crystal structure and complex model using bioinformatics and structural biology methods. This finding was consistent with a previous EMBO study that reported major contact between Axl^{-Ig1}-Gas6 and minor contact between Axl^{-Ig2}-Gas6 (23).

In the present study, the mAbs targeting the Axl^{-Ig1} functional domain were generated and evaluated in tumor cells with high Axl expression. Since anti-Axl mAb against the Axl^{-Ig1} domain was not commercially available, anti-Axl polyclonal antibody AF154 was used as the positive control to recognize the Axl^{-Ig1} domain for GST-Axl^{-Ig1} protein validation, clone screening and western blot analysis, as the Axl^{-Ig1} domain may be recognized by the polyclonal antibody, AF154 immunized by recombinant human Axl domain (33-440 aa; accession no. AAA61243), that overlaps with the Axl^{-Ig1} domain (27-128 aa). Furthermore, the first selective kinase inhibitor R428 (undergoing clinical phase II trials) (16-18) was selected as a positive control in the cell migration assays, since no neutralizing anti-Axl mAb is commercially available.

MDA-MB-231 is a highly invasive TNBC cell line with upregulated Axl expression (1,15). Consistent with previous reports (1,25,26), Axl was significantly upregulated in the MDA-MB-231 cell line without Gas6 stimulation and the phosphorylation of Axl was dependent on Gas6. Am1 or Am2 significantly reduced the protein expression level of Axl and almost completely blocked the stimulation of Gas6 in Axl phosphorylation and the Transwell migration assays, as well as producing similar activities to the positive control drug, R428, in the Transwell and wound healing migration assays. Thus, it was suggested that Am1 or Am2 attenuated MDA-MB-231 cell migration by blocking Axl signaling.

TNBC, accounting for 15-20% of breast cancer cases, is characterized by the absence of estrogen receptors, progesterone receptors and human epidermal growth factor receptor 2 (27,28). Due to the lack of therapeutic targets, no targeted therapy is currently available for TNBC. Fortunately, TNBC is sensitive to chemotherapy, which remains the most practicable therapeutic option for patients with TNBC (1,27). However, these patients remain susceptible to chemotherapy resistance (27,29,30).

An increasing number of studies have reported that the activation of Axl was associated with chemotherapy resistance in breast, colon, lung and other types of cancer (2,31-34). Therefore, Axl inhibitors can directly reduce tumor cell migration, as well as the development of chemotherapy resistance by blocking Axl activity. Previous studies have revealed that the Axl inhibitor, R428 enhanced the efficacy of chemotherapy by increasing the sensitivity of tumor cells to chemotherapeutic reagents in mesothelioma, uterine serous cancer and pancreatic cancer (9,13,14). Furthermore, the combination of chemotherapy and Axl inhibitors could improve clinical outcomes for patients, particularly those with TNBC, for which no targeted agents have been currently approved (1,26,35).

In addition, Axl has been associated with resistance not only to chemotherapy, but also to immunotherapy, targeted therapy and radiation therapy (2,11,36,37). The application of Axl inhibition combined with chemotherapy or targeted therapy has provided a promising treatment strategy for patients with breast and lung cancer (12,19,36,38).

Compared with the previous Axl-targeted mAbs, that are against Axl^{-ECD}, anti-Axl mAbs in the present study directly target Axl^{-Ig1}, the major Axl functional domain interacting with Gas6. To the best of our knowledge, no mAb that targets the Axl functional domain has been previously reported, which is the main advantage of the antibodies reported in the present study.

In conclusion, the present study investigated two anti-Axl mAbs targeting Axl^{-Ig1}, the major Axl functional domain interacting with Gas6. Anti-Axl mAbs almost completely neutralized the stimulation of Gas6 in Axl phosphorylation and cell migration assays, and displayed an almost similar activity to the positive control drug, R428 in the cell migration assays. Future studies are required to further evaluate the two anti-Axl mAbs for their bioactivity *in vitro* and *in vivo*, particularly in reducing the development of chemotherapy

resistance. The anti-Axl mAbs targeting the Axl^{-Ig1} domain might serve as an option for the combined therapy strategy.

Acknowledgements

Not applicable.

Funding

This study was supported by the National Natural Science Foundation of China (grant no. 31771010).

Availability of data and materials

The datasets used and/or analyzed in the current study are available from the first author upon reasonable request.

Authors' contributions

ML and JF designed the study. JF performed the computer-guided analysis. RA, XYL and XLL performed the experiments. HC and RA analyzed the data, drafted and revised the article. JF, ML and HC approved the version to be published. HC and ML confirm the authenticity of all the raw data. All authors have read and approved the final manuscript.

Ethics approval and consent to participate

The animal experiments were approved by the Animal Ethics Committee of Suzhou Vocational Health College (Jiangsu, China; approval no, SWAE201905).

Patient consent for publication

Not applicable.

Competing interests

The authors declare that they have no competing interests.

References

1. Leconet W, Chentouf M, du Manoir S, Chevalier C, Sirvent A, Ait-Arsa I, Busson M, Jarlier M, Radosevic-Robin N, Theillet C, *et al*: Therapeutic activity of anti-AXL antibody against triple-negative breast cancer patient-derived xenografts and metastasis. Clin Cancer Res 23: 2806-2816, 2017.
2. Gay CM, Balaji K and Byers LA: Giving AXL the axe: Targeting AXL in human malignancy. Br J Cancer 116: 415-423, 2017.
3. Duan Y, Luo L, Qiao C, Li X, Wang J, Liu H, Zhou T, Shen B, Lv M and Feng J: A novel human anti-AXL monoclonal antibody attenuates tumour cell migration. Scand J Immunol 90: e12777, 2019.
4. Myers SH, Brunton VG and Unciti-Broceta A: AXL inhibitors in cancer: A Medicinal Chemistry Perspective. J Med Chem 59: 3593-3608, 2016.
5. Colavito SA: AXL as a target in breast cancer therapy. J Oncol 2020: 5291952, 2020.
6. Leconet W, Larbouret C, Chardes T, Thomas G, Neiveyans M, Busson M, Jarlier M, Radosevic-Robin N, Pugniere M, Bernex F, *et al*: Preclinical validation of AXL receptor as a target for antibody-based pancreatic cancer immunotherapy. Oncogene 33: 5405-5414, 2014.
7. Iida S, Miki Y, Suzuki T, Mori K, Saito M, Niikawa H, Kondo T, Yamada-Okabe H and Sasano H: Activation of AXL and antitumor effects of a monoclonal antibody to AXL in lung adenocarcinoma. Anticancer Res 34: 1821-1827, 2014.
8. Wei J, Sun H, Zhang A, Wu X, Li Y, Liu J, Duan Y, Xiao F, Wang H, Lv M, *et al*: A novel AXL chimeric antigen receptor endows T cells with anti-tumor effects against triple negative breast cancers. Cell Immunol 331: 49-58, 2018.
9. Oien DB, Garay T, Eckstein S and Chien J: Cisplatin and pemetrexed activate AXL and AXL inhibitor BGB324 enhances mesothelioma cell death from chemotherapy. Front Pharmacol 8: 970, 2018.
10. Hong J, Peng D, Chen Z, Sehdev V and Belkhiri A: ABL regulation by AXL promotes cisplatin resistance in esophageal cancer. Cancer Res 73: 331-340, 2013.
11. Hong CC, Lay JD, Huang JS, Cheng AL, Tang JL, Lin MT, Lai GM and Chuang SE: Receptor tyrosine kinase AXL is induced by chemotherapy drugs and overexpression of AXL confers drug resistance in acute myeloid leukemia. Cancer Lett 268: 314-324, 2008.
12. Li Y, Ye X, Tan C, Hongo JA, Zha J, Liu J, Kallop D, Ludlam MJ and Pei L: Axl as a potential therapeutic target in cancer: Role of Axl in tumor growth, metastasis and angiogenesis. Oncogene 28: 3442-3455, 2009.
13. Palisoul ML, Quinn JM, Schepers E, Hagemann IS, Guo L, Reger K, Hagemann AR, McCourt CK, Thaker PH, Powell MA, *et al*: Inhibition of the receptor tyrosine kinase AXL restores paclitaxel chemosensitivity in uterine serous cancer. Mol Cancer Ther 16: 2881-2891, 2017.
14. Ludwig KF, Du W, Sorrelle NB, Wnuk-Lipinska K, Topalovski M, Toombs JE, Cruz VH, Yabuuchi S, Rajeshkumar NV, Maitra A, *et al*: Small-molecule inhibition of axl targets tumor immune suppression and enhances chemotherapy in pancreatic cancer. Cancer Res 78: 246-255, 2018.
15. Shen Y, Chen X, He J, Liao D and Zu X: Axl inhibitors as novel cancer therapeutic agents. Life Sci 198: 99-111, 2018.
16. Falcone I, Conciatori F, Bazzichetto C, Bria E, Carbognin L, Malaguti P, Ferretti G, Cognetti F, Milella M and Ciuffreda L: AXL receptor in breast cancer: Molecular involvement and therapeutic limitations. Int J Mol Sci 21: 8419, 2020.
17. Sheridan C: First Axl inhibitor enters clinical trials. Nat Biotechnol 31: 775-776, 2013.
18. Chen F, Song Q and Yu Q: Axl inhibitor R428 induces apoptosis of cancer cells by blocking lysosomal acidification and recycling independent of Axl inhibition. Am J Cancer Res 8: 1466-1482, 2018.
19. Ye X, Li Y, Stawicki S, Couto S, Eastham-Anderson J, Kallop D, Weimer R, Wu Y and Pei L: An anti-Axl monoclonal antibody attenuates xenograft tumor growth and enhances the effect of multiple anticancer therapies. Oncogene 29: 5254-5264, 2010.
20. Koopman LA, Terp MG, Zom GG, Janmaat ML, Jacobsen K, Gresnigt-van den Heuvel E, Brandhorst M, Forssmann U, de Bree F, Pencheva N, *et al*: Enapotamab vedotin, an AXL-specific antibody-drug conjugate, shows preclinical antitumor activity in non-small cell lung cancer. JCI Insight 4: e128199, 2019.
21. Ahnert JR, Taylor MH, O'Reilly E, Zhang J, Doebele R, Ben Y, Sharp L, Boyle WJ, Chang CY, Frey G, *et al*: A phase 1/2 dose-escalation and expansion study of a conditionally active anti-AXL humanized monoclonal antibody (BA3011) in patients with advanced solid tumors. J Clin Oncol 36 (Suppl 15): TPS12126, 2018.
22. Duan Y, Hu B, Qiao C, Luo L, Li X, Wang J, Liu H, Zhou T, Shen B, Lv M and Feng J: Engineered AXL^{-ECD}-Fc variants that abolish the AXL/Gas6 interaction suppress tumor cell migration. Oncol Lett 17: 5784-5792, 2019.
23. Sasaki T, Knyazev PG, Clout NJ, Cheburkin Y, Gohring W, Ullrich A, Timpl R and Hohenester E: Structural basis for Gas6-Axl signalling. EMBO J 25: 80-87, 2006.
24. Suzuki K, Nakamura K, Kato K, Hamada H and Tsukamoto T: Exploration of target molecules for prostate cancer gene therapy. Prostate 67: 1163-1173, 2007.
25. Wilson C, Ye X, Pham T, Lin E, Chan S, McNamara E, Neve RM, Belmont L, Koeppen H, Yauch RL, *et al*: AXL inhibition sensitizes mesenchymal cancer cells to antimitotic drugs. Cancer Res 74: 5878-5890, 2014.
26. D'Alfonso TM, Hannah J, Chen Z, Liu Y, Zhou P and Shin SJ: Axl receptor tyrosine kinase expression in breast cancer. J Clin Pathol 67: 690-696, 2014.
27. Nakhjavani M, Hardingham JE, Palethorpe HM, Price TJ and Townsend AR: Druggable molecular targets for the treatment of triple negative breast cancer. J Breast Cancer 22: 341-361, 2019.
28. Tovey H and Cheang MCU: Identifying biomarkers to pair with targeting treatments within triple negative breast cancer for improved patient stratification. Cancers (Basel) 11: 1864, 2019.
29. Carey L, Winer E, Viale G, Cameron D and Gianni L: Triple-negative breast cancer: Disease entity or title of convenience? Nat Rev Clin Oncol 7: 683-692, 2010.

30. Ding L, Gu H, Xiong X, Ao H, Cao J, Lin W, Yu M, Lin J and Cui Q: MicroRNAs involved in carcinogenesis, prognosis, therapeutic resistance and applications in human triple-negative breast cancer. Cells 8: 1492, 2019.
31. Kim KC, Baek SH and Lee C: Curcumin-induced downregulation of Axl receptor tyrosine kinase inhibits cell proliferation and circumvents chemoresistance in non-small lung cancer cells. Int J Oncol 47: 2296-2303, 2015.
32. Asiedu MK, Beauchamp-Perez FD, Ingle JN, Behrens MD, Radisky DC and Knutson KL: AXL induces epithelial-to-mesenchymal transition and regulates the function of breast cancer stem cells. Oncogene 33: 1316-1324, 2014.
33. Heckmann D, Maier P, Laufs S, Li L, Sleeman JP, Trunk MJ, Leupold JH, Wenz F, Zeller WJ, Fruehauf S and Allgayer H: The disparate twins: A comparative study of CXCR4 and CXCR7 in SDF-1α-induced gene expression, invasion and chemosensitivity of colon cancer. Clin Cancer Res 20: 604-616, 2014.
34. Sun ZG, Liu JH, Zhang JM and Qian Y: Research progress of Axl inhibitors. Curr Top Med Chem 19: 1338-1349, 2019.
35. Yang PW, Liu YC, Chang YH, Lin CC, Huang PM, Hua KT, Lee JM and Hsieh MS: Cabozantinib (XL184) and R428 (BGB324) inhibit the growth of esophageal squamous cell carcinoma (ESCC). Front Oncol 9: 1138, 2019.
36. Zhang ZF, Lee JC, Lin L, Olivas V, Au V, LaFramboise T, Abdel-Rahman M, Wang X, Levine AD, Rho JK, *et al*: Activation of the AXL kinase causes resistance to EGFR-targeted therapy in lung cancer. Nat Genet 44: 852-860, 2012.
37. Schoumacher M and Burbridge M: Key Roles of AXL and MER receptor tyrosine kinases in resistance to multiple anticancer therapies. Curr Oncol Rep 19: 19, 2017.
38. Liu L, Greger J, Shi H, Liu Y, Greshock J, Annan R, Halsey W, Sathe GM, Martin AM and Gilmer TM: Novel mechanism of lapatinib resistance in HER2-positive breast tumor cells: Activation of AXL. Cancer Res 69: 6871-6878, 2009.